DOI: 10.1021/ic100796e

Inorganic Chemistry
Article

Magnetic Ordering in Two Molecule-Based (10,3)-a Nets Prepared from a Copper(II) Trinuclear Secondary Building Unit

Beatriz Gil-Hernández,[†,‡] Pedro Gili,[†,§] Jana K. Vieth,[⊥,¶] Christoph Janiak,*[,⊥] and Joaquín Sanchiz*[,†]

[†]*Departamento de Química Inorgánica, Universidad de La Laguna, c/o Astrofísico Francisco Sánchez s/n, 38206 La Laguna, Spain, and* [⊥]*Institut für Anorganische und Analytische Chemie, Universität Freiburg, Albertstrasse 21, 79104 Freiburg, Germany.* [‡]*E-mail: beagh16@hotmail.com.* [§]*E-mail: pgili@ull.es.* [¶]*E-mail: jana.vieth@ac.uni-freiburg.de.*

Received April 23, 2010

Two new molecule-based materials of formulas 3D-$\{[K(H_2O)_6]_{0.5}[K(18\text{-crown-6})]_{0.5}[MnCu_3(Hmesox)_3]\cdot 5.25H_2O\}$ (**1**) and 3D-$\{(Ph_4P)_2[MnCu_3(Hmesox)_3Cl]\cdot 3.5H_2O\}$ (**2**) have been prepared from a tricopper(II) secondary building unit (SBU), $[Cu_3(Hmesox)_3]^{3-}$ (H_4mesox = mesoxalic acid, 2-dihydroxymalonic acid). Compound **1** is obtained by means of the reaction of the SBU with manganese(II) acetate in the presence of potassium cations and the 18-crown-6 ether, whereas compound **2** is obtained by means of the reaction of the SBU with manganese(II) acetate in the presence of Ph_4PCl. The $[MnCu_3(Hmesox)_3]^-$ and $[MnCu_3(Hmesox)_3Cl]^{2-}$ moieties in compounds **1** and **2**, respectively, yield chiral 3-connected three-dimensional (3D) anionic (10,3)-a (srs, $SrSi_2$) nets. In the cubic and centrosymmetric structures ($Pa\bar{3}$) of **1**, two inversion-symmetry-related anion nets interpenetrate to a racemic structure. The Ph_4P^+ cations in **2** are organized in a supramolecular (10,3)-a net through the 6-fold phenyl embrace. In **2**, both the cationic and anionic nets are homochiral and enantiopure with opposite handedness and form interpenetrating supramolecular and covalent (10,3)-a nets in the noncentrosymmetric Sohncke space group $P2_12_12_1$. Both compounds display ferrimagnetic interaction with long-range magnetic ordering below 2.5 and 15.2 K for **1** and **2**, respectively. A dehydrated phase of **2** exhibits a T_c of 21.8 K. The saturation of magnetization, M_S, indicates two different ground states, $S = {}^1/_2$ and ${}^3/_2$, for the tricopper(II) units in **1** and **2**, respectively. The different spin states of the tricopper(II) unit in **1** and **2** has been explained by means of a density functional theory (DFT) study performed in the $[Cu_3(Hmesox)_3]^{3-}$ and $[Cu_3(Hmesox)_3Cl]^{4-}$ fragments, for **1** and **2**, respectively. A further DFT study has allowed one to analyze the structural parameters that lead to the different spin ground states for the trinuclear units in both compounds.

Introduction

Magnetic ordering is a cooperative phenomenon that arises from an effective magnetic coupling of the paramagnetic centers through the bridging groups along the crystal framework.[1−12] The success in the consecution of this kind of behavior is directly related to the right selection of the building blocks, looking not only into their magnetic features (total spin and magnetic coupling) but also into the way they assemble altogether in the construction of the

*To whom correspondence should be addressed. E-mail: janiak@uni-freiburg.de (C.J.), jsanchiz@ull.es (J.S.). Tel: +49 761 2036127 (C.J.), +34 922 316502, ext 5425 (J.S.).

(1) de Jongh, L. J. In *Magneto-Structural Correlations in Exchange-Coupled Systems*; NATO-ASI Series C-140; Willett, R. D., Gatteschi, D., Kahn, O., Eds.; de Reidel: Dordrecht, The Netherlands, 1983; p 1−36.

(2) *Magnetism: A Supramolecular Function*; NATO ASI Series C-484; Kahn, O., Ed.; Kluwer Academic Publisher: Dordrecht, The Netherlands, 1996.

(3) (a) *Molecular Magnetism: From Molecular Assemblies to the Devices*; NATO-ASI Series E-321; Coronado, E., Delhaes, P., Gatteschi, D., Miller, J. S., Eds.; Kluwer Academic Publishers: Dordrecht, The Netherlands, 1996. (b) Shatruk, M.; Avendano, C.; Dunbar, K. R. *Prog. Inorg. Chem.* **2009**, *56*, 155. (c) Gatteschi, D.; Sessoli, R.; Villain, J. *Molecular Nanomagnets*; Oxford University Press: Oxford, U.K., 2006; references cited therein.

(4) Mrozinski, J. *Coord. Chem. Rev.* **2005**, *249*, 2534–2548.

(5) Decurtins, S.; Pelleaux, R.; Antorrena, G.; Palacio, F. *Coord. Chem. Rev.* **1999**, *190−192*, 841–854.

(6) (a) Coronado, E.; Clemente-León, M.; Galán-Mascarós, J. R.; Giménez-Saiz, C.; Gómez-García, C. J.; Martinez-Ferrero, E. *J. Chem. Soc., Dalton Trans.* **2000**, 3955. (b) Coronado, E.; Galán-Mascarós, J. R.; Martí-Gastaldo, C. *CrystEngComm* **2009**, *11*, 2143. (c) Bogani, L.; Vindigni, A.; Sessoli, R.; Gatteschi, D. *J. Mater. Chem.* **2008**, *18*, 4750. (d) Coronado, E.; Galán-Mascarós, J. R.; Martí-Gastaldo, C. *J. Am. Chem. Soc.* **2008**, *130*, 14987.

(7) (a) Long, J.; Chamoreau, L. M.; Marvaud, V. *Dalton Trans.* **2010**, *39*, 2188. (b) Bleuzen, A.; Marvaud, V.; Mothonière, C.; Sieklucka, B.; Verdaguer, M. *Inorg. Chem.* **2009**, *48*, 3453. (c) Verdaguer, M.; Bleuzen, A.; Marvaud, V.; Vaissermann, J.; Seuleiman, M.; Desplanches, C.; Scuiller, A.; Train, C.; Garde, R.; Gelly, G.; Lomenech, C.; Rosenman, I.; Veillet, P.; Cartier, C.; Villain, F. *Coord. Chem. Rev.* **1999**, *190−192*, 1023.

(8) (a) Dul, M. C.; Pardo, E.; Lescouëzec, R.; Journaux, Y.; Ferrando-Soria, J.; Ruiz-García, R.; Cano, J.; Julve, M.; Lloret, F.; Cangussu, D.; Pereira, C. L. M.; Stumpf, H.; Pasán, J.; Ruiz-Pérez, C. *Coord. Chem. Rev.* **2010**, DOI:10.1016/j.ccr.2010.03.003. (b) Ruiz, R.; Faus, J.; Lloret, F.; Julve, M.; Journaux, Y. *Coord. Chem. Rev.* **1999**, *193−195*, 1069.

(9) Pilkington, M.; Decurtins, S. In *Comprenhensive Coordination Chemistry II: From Biology to Nanotechnology*; McCleverty, J. A., Ed, T. J. M., Eds.; Elsevier: Oxford, U.K., 2004; Vol. *7*, p 177.

Published on Web 07/21/2010

Scheme 1. Schematic Structure of Mesoxalic or Dihydroxymalonic Acid (H_4mesox)

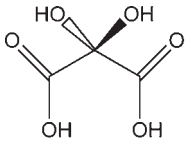

mesoxalic acid,
dihydroxymalonic acid

Scheme 2. Tris-bidentate Bridging Ligands and 3-Connected Mn^{2+} Nodes as SBUs for 3-Connected 3D Nets

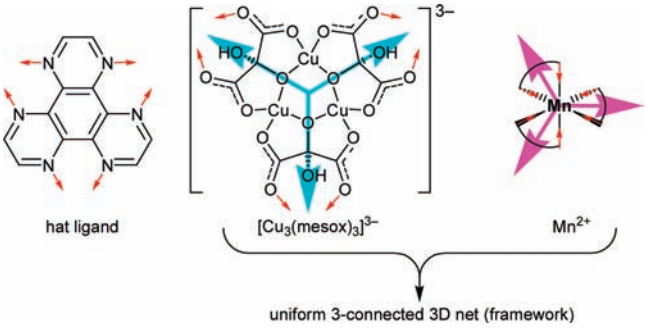

crystal network. The so-called reticular synthesis is then an important concept for the preparation of molecule-based magnets.[5,12−16] The intensity and the ferro- or antiferromagnetic nature of the magnetic interaction among the spin carriers has been deeply investigated and now is well understood, with the characteristics of the couplings among paramagnetic centers being easy to predict through a particular bridging group.[11] Also, recent extensive research into the design and synthesis of metal−organic frameworks (MOFs) has led to numerous practical and conceptual developments in this direction that have allowed a considerable increase in the predictability of the synthesis.[5,14−18] Thus, a rational synthesis of a molecule-based magnet starts with an evaluation of the structural and magnetic features of the selected components.

We investigate here the secondary building unit (SBU) or metalloligand features of the trinuclear complex $[Cu_3(Hmesox)_3]^{3-}$, which is formed by the trianion of mesoxalic acid (Scheme 1) with copper(II). In the planar, 3-connecting, bridging $[Cu_3(Hmesox)_3]^{3-}$ SBU (Scheme 2), the mesoxalato exhibits a very suitable configuration of the bridging groups

Scheme 3. Bridging Scheme of the Mesoxalato Complexes[a]

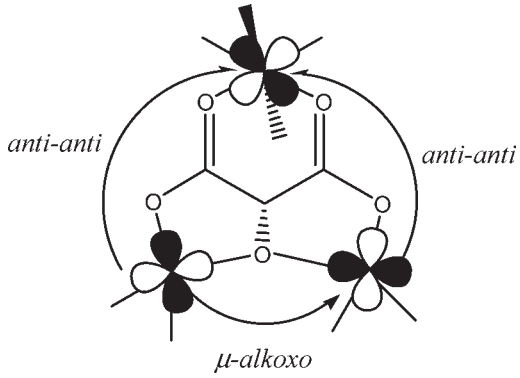

[a] An −OH group is omitted for clarity.

to mediate effectively the magnetic coupling toward external 3d or 4f paramagnetic ions through the anti−anti bridging mode of the carboxylate groups (Scheme 3).[19] Moreover, its trinuclear character gives a nonzero spin state at any T.[20−30]

This paramagnetic trinuclear anion has an almost planar structure, and its arrangement of the carboxylate groups allows it to act as a tris-bidentate connector (Scheme 2). Triangular and 3-connected SBUs are able to form three-dimensional (3D) networks, as predicted by Wells.[31] The established planar ligand 1,4,5,8,9,12-hexaazatriphenylene (hat)[17] provides a similar symmetric array of three bidentate sites at which metal centers can be bound to yield 3D [(10,3)-a] networks with metal ions acting as 3-connecting nodes.[5,14−16,31−34]

The paramagnetic ($S = {}^5/_2$) Mn^{II} ion can act as a 3-connecting node in octahedral or distorted octahedral geometry toward rigid bidentate ligands, such as oxalate, malonate, or 2,2′-bipyridine and derivatives.[35] The combination of its paramagnetism and its 3-connecting behavior makes it a

(10) (a) Vallejo, J.; Castro, I.; Cañadillas-Delgado, L.; Ruiz-Pérez, C.; Ferrando-Soria, J.; Ruiz-García, R.; Cano, J.; Lloret, F.; Julve, M. *Dalton Trans.* **2010**, *39*, 2350. (b) Clemente-León, M.; Coronado, E.; López-Jordá, M.; Mínguez-Espallargas, G.; Soriano-Portillo, A.; Waerenborgh, J. C. *Chem.—Eur. J.* **2010**, *16*, 2207. (c) Martínez-Lillo, J.; Armentano, D.; De Munno, G.; Wernsdorfer, W.; Clemente-Juan, J. M.; Krzystek, J.; Lloret, F.; Julve, M.; Faus, J. *Inorg. Chem.* **2009**, *48*, 3027. (d) Ohba, M.; Okawa, H. *Coord. Chem. Rev.* **2000**, *198*, 313.
(11) Kahn, O. *Molecular Magnetism*; VCH: New York, 1993.
(12) Pardo, E.; Ruiz-Garcia, R.; Cano, J.; Ottenwaelder, X.; Lescouezec, R.; Journaux, Y.; Lloret, F.; Julve, M. *Dalton Trans.* **2008**, 2780–2805.
(13) Yaghi, O. M.; O'Keeffe, M.; Ockwig, N. W.; Chae, H. K.; Eddaoudi, M.; Kim, J. *Nature* **2003**, *423*, 705–714.
(14) Clément, R.; Decurtins, S.; Gruselle, M.; Train, C. *Monatsh. Chem./Chem. Monthly* **2003**, *134*, 117–135.
(15) Pilkington, M.; Gross, M.; Franz, P.; Biner, M.; Decurtins, S.; Stoeckli-Evans, H.; Neels, A. *J. Solid State Chem.* **2001**, *159*, 262–267.
(16) Decurtins, S.; Schmalle, H. W.; Schneuwly, P.; Pelleaux, R.; Ensling, J. *Mol. Cryst. Liq. Cryst.* **1995**, *273*, 167–174.
(17) Robson, R. *J. Chem. Soc., Dalton Trans.* **2000**, 3735.
(18) Janiak, C. *Dalton Trans.* **2003**, 2781–2804.
(19) Abrahams, B. F.; Hudson, T. A.; Robson, R. *J. Mol. Struct.* **2006**, *796*, 2–8.
(20) Dul, M. C.; Ottenwaelder, X.; Pardo, E.; Lescouëzec, R.; Journaux, Y.; Chamoreau, L. M.; Ruiz-García, R.; Cano, J.; Julve, M.; Lloret, F. *Inorg. Chem.* **2009**, *48*, 5244–5249.
(21) Ferrer, S.; Lloret, F.; Bertomeu, I.; Alzuet, G.; Borrás, J.; García-Granada, S.; Liu-González, M.; Haasnoot, J. G. *Inorg. Chem.* **2002**, *41*, 5821–5830.
(22) Afrati, T.; Dendrinou-Samara, C.; Raptopoulou, C. P.; Terzis, A.; Tangouilis, V.; Tsipis, A.; Kessissoglou, P. *Inorg. Chem.* **2008**, *47*, 7545.
(23) González-Alvarez, A.; Alfonso, I.; Cano, J.; Díaz, P.; Gotor, V.; Gotor-Fernández, V.; García-España, E.; García-Granada, S.; Jiménez, H. R.; Lloret, F. *Angew. Chem., Int. Ed.* **2009**, *48*, 6055–6058.
(24) Yoon, J.; Solomon, E. I. *Inorg. Chem.* **2005**, *44*, 8076–8086.
(25) Afrati, T.; Dendrinou-Samara, C.; Raptopoulou, C.; Terzis, A.; Tangoulis, V.; Kessissoglou, D. P. *Dalton Trans.* **2007**, 5156–5164.
(26) Liu, X.; de Miranda, M. P.; McInnes, E. J. L.; Kilner, C. A.; Halcrow, M. A. *Dalton Trans.* **2004**, 59–64.
(27) Mirica, L. M.; Stack, T. D. P. *Inorg. Chem.* **2005**, *44*, 2131–2133.
(28) Gautier-Luneau, I.; Phanon, D.; Duboc, C.; Luneau, D.; Pierre, J. L. *Dalton Trans.* **2005**, 3795–3799.
(29) Lopez-Sandoval, H.; Contreras, R.; Escuer, A.; Vicente, R.; Bernès, S.; Nöth, H.; Leigh, G. J.; Barba-Behrens, N. *J. Chem. Soc., Dalton Trans.* **2002**, 2648–2653.
(30) Yoon, J.; Solomon, E. I. *Coord. Chem. Rev.* **2007**, *251*, 379–400.
(31) Wells, A. F. *Three Dimensional Nets and Polyhedra*; Wiley: New York, 1977.
(32) Robson, R. *Dalton Trans.* **2008**, 5113–5131.
(33) Shatruck, M.; A. Chouai, A.; Dunbar, K. R. *Dalton Trans.* **2006**, 2184–2191.
(34) Abrahams, F. B.; Jackson, P. A.; Robson, R. *Angew. Chem., Int. Ed.* **1998**, *37*, 2656.
(35) Sauvage, J. P. *Transition Metals in Supramolecular Chemistry*; Wiley: New York, 1999; Vol. *5*.

good building unit for the preparation of extended 3D paramagnetic networks.[36]

The (10,3)-a net is a typical and frequent net of two 3-connecting nodes (cf. Figure 3)[37−45] and, as its alternative description as an $SrSi_2$ (srs) net shows, is also observed in solid-state compounds.[46,47] Additionally, if the 3-connectors are paramagnetic and efficient in the transmission of the magnetic effect, they may also lead to a long-range magnetic ordering in the 3D nets.[5,14−16] Examples of (10,3)-a nets with antiferromagnetic coupling,[48−51] alternating ferro- and antiferromagnetic interaction,[52] or spin crossover[53] have been described. Thus, the planar 3-connecting, bridging $[Cu_3(Hmesox)_3]^{3-}$ metalloligands combined with the 3-connecting Mn^{2+} (or other M'^{n+}) nodes can lead to different types of 3D nets, which may exhibit interesting properties such as long-range magnetic ordering, chirality, magnetochirality, porosity, or interpenetration.[17,18,36,54] Following this strategy and as a continuation of our work in the study of the magnetic properties of paramagnetic clusters[55−57] and MOFs,[58−67] we prepared 3D-{$[K(H_2O)_6]_{0.5}[K(18\text{-crown-}6)]_{0.5}[MnCu_3(Hmesox)_3]\cdot 5.25H_2O$} (**1**) and 3D-{$(Ph_4P)_2[MnCu_3(Hmesox)_3Cl]\cdot 3.5H_2O$} (**2**). We describe herein their structures and magnetic behavior, showing interesting properties and therefore a validation of the strategy.

Experimental Section

Materials. Basic copper carbonate $CuCO_3\cdot Cu(OH)_2$, manganese(II) acetate tetrahydrate, mesoxalic acid, potassium chloride, tetraphenylphosphonium chloride, 1,4,7,10,13,16-hexaoxacyclooctadecane (18-crown-6 ether), methanol, ethanol, and diethyl ether were purchased from commercial sources and used as received.

3D-{$[K(H_2O)_6]_{0.5}[K(18\text{-c-}6)]_{0.5}[MnCu_3(Hmesox)_3]\cdot 5.25H_2O$} (1). To a solution of mesoxalic acid (136 mg, 1 mmol) in water (2 mL) is added in small portions solid basic copper(II) carbonate (110 mg, 0.5 mmol), allowing the CO_2 to evolve before adding a new portion. The reaction is performed at 30−40 °C in a water bath for 10 min. When the reaction is finished, the solution is filtered and diluted to 10 mL by the addition of distilled water. An aqueous solution of manganese(II) acetate (82 mg, 0.33 mmol in 2 mL of water) is then added to the clear blue solution and finally a water−methanolic solution of KCl (149.2 mg, 2 mmol in 2 mL of water) and 18-crown-6 (530 mg, 2 mmol in 2 mL of methanol). Single crystals of **1** were obtained by slow evaporation at 21 °C within 10 days. The crystals are filtered and washed with water and dried in an air current. Yield: 161 mg, 49.9%. Elem anal. Calcd for $C_{15}H_{31.50}Cu_3KMnO_{29.25}$ (964.56): C, 18.68; H, 3.28. Found: C, 18.81; H, 3.06. IR (400−4000 cm^{-1}): The most intense bands are those of the ν_{as} and ν_s carboxylate groups at 1601 and 1369, respectively. Also, those of the 18-crown-6 ether (2922, 2879, 1445, 1103, 950, and 822 cm^{-1}) are observed.

3D-{$(Ph_4P)_2[MnCu_3(Hmesox)_3Cl]\cdot 3.5H_2O$} (2). Compound **2** is obtained in a manner similar to that of **1** except adding an aqueous solution of Ph_4PCl (250 mg, 0.66 mmol in 1 mL of water) instead of KCl and 18-crown-6 ether. The solution is allowed to crystallize at room temperature. Single crystals of **2** separate from the mother liquor within 1 week. The crystals are filtered, washed with ethanol and diethyl ether, and dried under an air current for 15 min at room temperature. Yield: 148 mg, 32%. The single crystals for determination of the crystal structure did not follow the drying procedure and were mounted directly from the mother liquor. Elem anal. Calcd for $C_{57}H_{50}ClCu_3MnO_{21.5}P_2$ (1421.88): C, 48.13; H, 3.51. Found: C, 48.18; H, 3.53. IR (400−4000 cm^{-1}): The most intense bands are those of the tetraphenylphosphonium cation (1609, 1586, 1481, 1437, 11081, 990, 723, 690, 528 cm^{-1}) that overlap with the ν_{as} and ν_s of the carboxylate groups [1650−1550 (s, b) and 1390 (s) cm^{-1}, respectively]. The C−O stretching bands are observed at 1391 and 1124 (s) cm^{-1}. The thermogravimetric analysis (TGA) of **2** shows a mass loss percentage of 4.5% in the temperature range 25−140 °C, corresponding to a loss of 3.5 weakly bound crystallization water molecules. A progressive weight loss occurs upon further heating that consists of degradation of the organic part of the material (Figure S1 in the Supporting Information).

Physical Techniques. Elemental analyses (C and H) were performed on a FLASH EA 1112 CHNS-O microanalytical analyzer. IR spectra (400−4000 cm^{-1}) were recorded on a Thermo Nicolet Avatar 360 FT-IR spectrometer with the

(36) Wells, A. F. *Structural Inorganic Chemistry*; Oxford University Press: New York, 1984.
(37) Oehrstroem, L.; Larsson, K. *Dalton Trans*. **2004**, 347–353.
(38) Liu, Y. J.; Huang, J. S.; Chui, S. S.; Li, C. H.; Zuo, J. L.; Zhu, N.; Che, C. M. *Inorg. Chem*. **2008**, *47*, 11514–11518.
(39) Tang, Y.; Tang, K. Z.; Liu, W. S.; Tan, M. Y. *Sci. China, Ser. B: Chemistry* **2008**, *51*, 614–622.
(40) Ma, S.; Fillinger, J. A.; Ambrogio, M. W.; Zuo, J. L.; Zhou, H. C. *Inorg. Chem. Commun*. **2007**, *10*, 220–222.
(41) Tang, Y.; Zhang, J.; Liu, W. S.; Tan, M. Y.; Yu, K. B. *Polyhedron* **2005**, *24*, 1160–1166.
(42) Sumby, C. J.; Hardie, M. J. *Cryst. Growth Des*. **2005**, *5*, 1321–1324.
(43) Bu, X. H.; Chen, W.; Du, M.; Biradha, K.; Wang, W. Z.; Zhang, R. H. *Inorg. Chem*. **2002**, *41*, 437–439.
(44) Kheradmandan, S.; Schmalle, H. W.; Jacobsen, H.; Blacque, O.; Fox, T.; Berke, H.; Gross, M.; Decurtins, S. *Chem.—Eur. J*. **2002**, *8*, 2526–2533.
(45) Ohrstrom, L.; Larsson, K.; Borg, S.; Norberg, S. T. *Chem.—Eur. J*. **2001**, *7*, 4805–4810.
(46) Evers, J.; Oehlinger, G.; Polborn, K.; Sendlinger, B. *J. Solid State Chem*. **1993**, *103*, 45–56.
(47) Evers, J.; Oehlinger, G.; Polborn, K.; Sendlinger, B. *J. Solid State Chem*. **1991**, *91*, 250–263.
(48) Tynan, E.; Jensen, P.; Kelly, N. R.; Kruger, P. E.; Lees, A. C.; Moubaraki, B.; Murray, K. S. *Dalton Trans*. **2004**, 3440–3447.
(49) Dai, Y.; Shi, W.; Zhu, X. J.; Zhao, B.; Cheng, P. *Inorg. Chim. Acta* **2006**, *359*, 3353–3358.
(50) Zhang, W. X.; Xue, W.; Lin, J. B.; Zheng, Y. Z.; Chen, X. M. *CrystEngComm* **2008**, *10*, 1770–1776.
(51) Pointillart, F.; Train, C.; Gruselle, M.; Villain, H.; Schmalle, H. W.; Talbot, D. P. G.; Decurtins, S.; Verdaguer, M. *Chem. Mater*. **2004**, *16*, 832–841.
(52) Liu, C. M.; Gao, S.; Zhang, D. Q.; Huang, Y. H.; Xiong, R. G.; Liu, Z. L.; Jiang, F. C.; Zhu, D. B. *Angew. Chem., Int. Ed*. **2004**, *43*, 990–990.
(53) Sieber, R.; Decurtins, S.; Stoeckli-Evans, H.; Wilson, C.; Yufit, D.; Howard, J. A. K.; Capeli, S. C.; Hauser, A. *Chem.—Eur. J*. **2000**, *6*, 361–368.
(54) (a) Rikken, G. L. J. A.; Raupach, E. *Nature* **1997**, *390*, 493. (b) Raupach, E.; Rikken, G. L. J. A.; Train, C.; Maléizieux, B. *Chem. Phys*. **2000**, *261*, 535. (c) Rikken, G. L. J. A.; Raupach, E. *Nature* **2000**, *405*, 932.
(55) Monfared, H. H.; Sanchiz, J.; Kalantari, Z.; Janiak, C. *Inorg. Chim. Acta* **2009**, *362*, 3791–3795.
(56) Habib, H. A.; Sanchiz, J.; Janiak, C. *Dalton Trans*. **2008**, 1734–1744.
(57) Ruiz-Pérez, C.; Sanchiz, J.; Hernández-Molina, M.; Lloret, F.; Julve, M. *Inorg. Chem*. **2000**, *39*, 1363–1370.
(58) Delgado, F. S.; Ruiz-Pérez, C.; Sanchiz, J.; Lloret, F.; Julve, M. *CrystEngComm* **2006**, *8*, 507–529.
(59) Delgado, F. S.; Ruiz-Pérez, C.; Sanchiz, J.; Lloret, F.; Julve, M. *CrystEngComm* **2006**, *8*, 530–544.
(60) Delgado, F. S.; Hernández-Molina, M.; Sanchiz, J.; Ruiz-Pérez, C.; Rodríguez-Martín, Y.; López, T.; Lloret, F.; Julve, M. *CrystEngComm* **2004**, *6*, 106–111.
(61) Delgado, F. S.; Sanchiz, J.; Ruiz-Pérez, C.; Lloret, F.; Julve, M. *CrystEngComm* **2004**, *6*, 443–450.
(62) Rodríguez-Martín, Y.; Hernández-Molina, M.; Sanchiz, J.; Ruiz-Pérez, C.; Lloret, F.; Julve, M. *Dalton Trans*. **2003**, 2359.
(63) Pasán, J.; Sanchiz, J.; Lloret, F.; Julve, M.; Ruiz-Pérez, C. *CrystEngComm* **2007**, *9*, 478.
(64) Pasán, J.; Sanchiz, J.; Ruiz-Pérez, C.; Campo, J.; Lloret, F.; Julve, M. *Chem. Commun*. **2006**, 2857–2859.
(65) Pasán, J.; Sanchiz, J.; Ruiz-Pérez, C.; Lloret, F.; Julve, M. *Inorg. Chem*. **2005**, *44*, 7794–7801.
(66) Pasán, J.; Sanchiz, J.; Ruiz-Pérez, C.; Lloret, F.; Julve, M. *Eur. J. Inorg. Chem*. **2004**, 4081–4090.
(67) Pasán, J.; Sanchiz, J.; Ruiz-Pérez, C.; Lloret, F.; Julve, M. *New J. Chem*. **2003**, *27*, 1557–1562.

sample prepared as KBr pellets. Thermal analysis was carried out on a Perkin-Elmer system (model Pyris Diamond TG/DTA) under a nitrogen atmosphere (flow rate: 80 $cm^3\ min^{-1}$) from 25 to 750 °C at a heating rate of 5 °C min^{-1}. Magnetic susceptibility measurements on polycrystalline samples were carried out by means of a Quantum Design SQUID magnetometer. In order to avoid the loss of crystallization water molecules of compound **2**, the sample was inserted in the sample chamber at 110 K under a helium flow, and then the system was locked and purged several times for removal of dioxygen traces. The measurements were performed in the temperature range 1.9−300 K at direct-current applied fields of 50 Oe for $T < 50$ K and of 1000 Oe for $T > 35$ K. Alternating-current (ac) measurements were performed at various frequencies (1, 10, 100, 500, and 1000 Hz) with an ac field of 3 Oe and a static field of 0 Oe. Diamagnetic corrections of the constituent atoms were estimated from Pascal's constants, and experimental susceptibilities were also corrected for temperature-independent paramagnetism and magnetization of the sample holder.

Crystal Structure Determination. *Data Collection*: Bruker AXS with a CCD area detector, temperature 203(2) K, Mo Kα radiation ($\lambda = 0.710\,73$ Å), graphite monochromator, ω scans, data collection, and cell refinement with *SMART*,[68] data reduction with *SAINT*,[68] and experimental absorption correction with *SADABS*.[69] Despite numerous attempts, the crystals of **2** did not diffract to high θ angles, which may be traced to some disorder in the Ph_4P^+ cation orientation in the voids. *Structure Analysis and Refinement*: The structures were solved by direct methods (*SHELXS-97*),[70,71] and refinement was done by full-matrix least squares on F^2 using the *SHELXL-97* program suite.[70,71] All non-hydrogen positions in **2** and in the anion nets of **1** were refined with anisotropic temperature factors. In **1**, the water molecules of crystallization, respectively aqua ligands for two symmetry-independent hexaaquapotassium, $[K(H_2O)_6]^+$ groups with K1 and K2, are highly disordered. The positions K1 and K2 are only a quarter occupied each. K1 shares its position with the water of crystallization of O7. K2 shares its position with the water of crystallization of O9 (disordered in turn over O9a and O9b). The half-occupied potassium atom K3 of (18-crown-6)potassium, $[K(18\text{-c-}6)]^+$, is disordered over two positions, equally occupied, to either side of the disordered 18-crown-6 ligand. The carbon and oxygen atoms of the 18-crown-6 ring (i.e., the whole ring) are disordered. The disorder in the cations of **1** affects the overall crystal and data-set quality. Still, the anion net structure of **1** could be unequivocally determined. A 50:50 disorder to CuA and CuB and O1A and O1B atom positions in **1** does not affect the determination of the anion network structure. In the structure refinement of **2**, only one crystal water oxygen atom could be clearly identified. While the residual electron density is small (0.41 e $Å^{-3}$) and located within 1.5 Å of the phenyl rings, there may be additional crystal water molecules present in the voids, perhaps also with occupancies of less than 1. For the refined structure of compound **2**, *PLATON*[72−74] still calculates a total potential solvent volume of 114.0 $Å^3$ per unit cell volume of 5698 $Å^3$ (2.0%). This has to be compared to the expected volume for a hydrogen-bonded water molecule of 40 $Å^3$. In **1**, the hydrogen atoms on the crystal water oxygen atom could be neither found nor calculated because of the disorder problems. Also, the hydrogen atoms of the 18-crown-6 carbon atoms have not been calculated because of the severe ring disorder. The hydrogen atoms in **1** have only been included in the unit card for calculation of the correct sum formula, density, and $F(000)$ because of their large number. The phenyl rings of the Ph_4P^+ cations in **2** were refined with a rigid group constraint for the phenyl rings (AFIX 66) and restraining the anisotropic displacement parameters with a "similar U_{ij}" restraint (SIMU). Hydrogen atoms on the carbon atoms were positioned geometrically (C−H = 0.94 Å for aromatic CH) and refined using a riding model (AFIX 43 for aromatic CH) with $U_{iso}(H) = 1.2U_{eq}(CH)$. Hydrogen atoms on a crystal water oxygen atom in **2** could be neither found nor calculated. Details of the X-ray structure determinations and refinements are provided in Table 1. Graphics were drawn with *DIAMOND* (version 3.2c).[75] Network analysis was carried out using the program package *TOPOS*.[76,77] The structural data have been deposited with the Cambridge Crystallographic Data Center (CCDC 781994 for **1** and CCDC 781995 for **2**).

Computational Details. Spin-unrestricted density functional theory (DFT) calculations were performed at the B3LYP level by means of the *Gaussian03* code.[78] A triple-ξ all-electron Gaussian basis set was used for the copper[79] atoms and a 6-31G(d) basis set for the rest of the nonmetallic elements. Single-point calculations were performed for both the quartet, high-spin, HS, with $\langle S^2\rangle \approx 3.75$ states and the broken symmetry, BS, with $\langle S^2\rangle \approx 1.75$ states. The particular details for each calculation are given in the corresponding sections, and the atomic coordinates of all of the atoms of the calculated structures are given in the Supporting Information. In copper(II) cyclic trinuclear clusters with C_3 symmetry, the relative energies of the HS and BS states can be used to estimate the isotropic exchange constant, $J = -(E_{HS} - E_{BS})$, where E_{HS} and E_{BS} refer to the total energy of the HS and BS states, respectively (Scheme 4).[24] This equation assumes the following spin Hamiltonian for the trinuclear unit with C_3 symmetry:

$$\mathbf{H} = -J(S_1S_2 + S_2S_3 + S_3S_1) \qquad (1)$$

Result and Discussion

Crystal Structures. The cubic structure of **1** contains one unique copper atom and mesoxalato ligand; the orthorhombic structure of **2** contains three crystallographically different copper atoms and mesoxalato ligands. Each mesoxalato ligand is triply deprotonated, i.e., $C_3HO_6^{3-}$ and functions as a chelating and bridging ligand to and between two copper atoms and one manganese atom with a μ_3-κO:O′,O″:O′,O‴:O^{v} binding mode (Figure 1).

Only the hydroxyl group out of the six oxygen atoms in $C_3HO_6^{3-}$ is not involved in metal coordination. Each copper atom is chelated by two mesoxalato ligands to a five-membered chelate ring. The copper coordination is distorted square planar in **1**. In **2**, a chlorine atom bridges between three copper atoms with long Cu−Cl bonds (> 2.5 Å)

(68) *SMART, Data Collection Program for the CCD Area-Detector System* and *SAINT, Data reduction and Frame Integration Program for CCD Area-Detector System*; Bruker Analytical X-ray Systems: Madison, WI, 1997.

(69) Sheldrick, G. M., *Program SADABS: Area-detector absorption correction*; University of Göttingen: Göttingen, Germany, 1996.

(70) Sheldrick, G. M. *Acta Crystallogr., Ser. A* **2008**, *64*, 112–122.

(71) Sheldrick, G. M. *SHELXS-97 and SHELXL-97, Programs for Crystal Structure Analysis*; University of Göttingen: Göttingen, Germany, 1997.

(72) Spek, A. L. *Acta Crystallogr., Ser. A* **1990**, *46*, C34.

(73) Spek, A. L. *PLATON—A Multipurpose Crystallographic Tool*; Ultrecht University: Ultrecht , The Netherlands, 2006.

(74) Farrugia, L. J. *PLATON, Windows implementation*, version 29-10-07; University of Glasgow: Glasgow, Scotland, 1995−2006.

(75) Brandenburg, K. *Diamond, Crystal and Molecular Structure Visualization*, version 3.2c; Crystal Impact - K. Brandenburg & H. Putz Gbr: Bonn, Germany, 2009; http//www.Crystalimpact.com/diamond.

(76) Blatov, V. A. *IUCr Compcomm Newsletter* **2006**, *7*, 4; http://www.iucr.org/iucr-top/comm/ccom/newsletters.

(77) *TOPOS program package for multipurpose crsytallochemical analysis*, version 4.0; http://www.topos.ssu.samara.ru.

(78) Frisch, M. J. *Gaussian 03*; revision C.02; Gaussian. Inc.: Wallingford, CT, 2004.

(79) Scheafer, A.; Huber, C.; Ahlrichs, R. *J. Chem. Phys.* **1994**, *100*, 5829–5835.

Table 1. Crystal Data and Structure Refinement for **1** and **2**

	1	**2**
empirical formula	$C_{15}H_{31.50}Cu_3KMnO_{29.25}$ [a]	$C_{57}H_{45}ClCu_3MnO_{19}P_2$ [a,b]
fw	964.56	1376.88
cryst size (mm^3)	0.15 × 0.12 × 0.08	0.48 × 0.42 × 0.33
θ range for data collection (deg)	4.44−51.72	3.96−40.06
completeness to 2θ (%)	98.8 (99.2 for 50°)	99.8
h; k; l range	−22, 19; −20, 15; −19, 5	±16, ±17, ±17
cryst syst	cubic	orthorhombic
space group	$Pa\bar{3}$ (No. 205)	$P2_12_12_1$ (No. 19)
unit cell dimens		
a (Å)	18.346(2)	16.963(3)
b (Å)	18.346(2)	18.283(3)
c (Å)	18.346(2)	18.373(3)
V ($Å^3$)	6174.8(12)	5698.2(15)
Z	8	4
D_{calc} (Mg m^{-3})	2.075	1.605
$F(000)$	3892	2792
abs coeff μ (mm^{-1})	2.686	1.499
max/min transmn	0.8138/0.6887	0.6375/0.5331
reflns collected	7066	19510
indep reflns (R_{int})	1981 (0.1125)	5328 (0.0909)
no. of reflns used [$I > 2\sigma(I)$]	1167	3972
no. of param refined	181	652
max/min $\Delta\rho$/e $Å^{-3}$ [c]	0.437/−0.433	0.407/−0.365
final R indices		
R1/wR2 [$I > 2\sigma(I)$] [d]	0.0765/0.1467	0.0598/0.1473
R1/wR2 (all data) [d]	0.1446/0.1716	0.0866/0.1643
GOF [e]	1.072	1.022
wt scheme w; a/b [f]	0.0527/5.0478	0.0967/0.0000
absolute structure parameter (Flack value)[80−82]		0.00(3)

[a] Aqua, crystal water and 18-c-6 hydrogen atoms in **1** and crystal water hydrogen atoms in **2** could not be found or calculated, but the hydrogen atoms were included in the empirical formula and calculation of the molecular mass, density, and $F(000)$. [b] From *PLATON*,[72] void calculations, elemental analysis, and TGA, about 2−2.5 additional crystal water molecules (bringing the crystal water to 3−3.5H_2O in total) may be present in the voids that could not be located upon refinement (see the crystallography text). [c] Largest difference peak and hole. [d] $R1 = [\sum(||F_o| - |F_c||)/\sum|F_o|]$; $wR2 = [\sum[w(F_o^2 - F_c^2)^2]/\sum[w(F_o^2)^2]]^{1/2}$. [e] $GOF = [\sum[w(F_o^2 - F_c^2)^2]/(n-p)]^{1/2}$. [f] $w = 1/[\sigma^2(F_o^2) + (aP)^2 + bP]$, where $P = [\max(F_o^2 \text{ or } 0) + 2F_c^2]/3$.

Scheme 4. Magnetic Coupling Scheme of a Coupled Copper(II) Trinuclear Unit with C_3 Symmetry and Energy Splitting of the HS and BS States

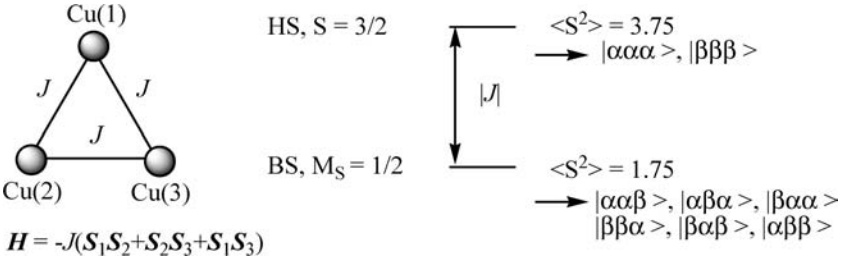

and complements a distorted square-pyramidal copper coordination sphere (see the τ parameters in Table 3).[83]

The structures of **1** and **2** agree in the assembly of the copper atoms and mesoxalato ligands to a trigonal metalloligand $\{Cu_3(C_3HO_6)_3\}^{3-}$ in **1** or $\{Cu_3(C_3HO_6)_3Cl\}^{4-}$ in **2** (Figure 2). This metalloligand then bridges between three symmetry-related manganese atoms. Each manganese atom is coordinated by three six-membered chelate rings of three symmetry-related mesoxalato or metalloligands (Figure 1).

The bridging action of manganese and the Cu_3 metalloligand gives a 3D anion framework, $[Mn\{Cu_3(C_3HO_6)_3\}]^-$ and $[Mn\{Cu_3(C_3HO_6)_3Cl\}]^{2-}$ in **1** and **2**, respectively. The network topology is $SrSi_2$, (10,3)-a with point (Schläfli) symbol 10^3 if the manganese atom and the Cu_3 centroid are considered as nodes (Figure 3).[31]

A single (10,3)-a net is homochiral.[5,14−16,37] The manganese atoms in **1** and **2** all have the same Λ or Δ configuration, respectively, within such a single net. If one traces the four-membered helices, one finds the same handedness within a (10,3)-a net. In the measured crystal of compound **2**, the trischelated manganese atoms assume the enantiopure Λ configuration (Figure 1) and the helices are all left-handed (*M*) (Figure 3). In the cubic and centrosymmetric structure of **1**, two inversion-symmetry-related anion nets interpenetrate (Figure 4). Thus, the two interpenetrated nets differ in their chirality at the manganese atoms and when one traces the opposite handedness in the four-membered helices, so that the overall structure of **1** is racemic.

The charge balance to the mononegative 3D anion framework (per formula unit) in **1** is derived by a half hexaaquapotassium, $[K(H_2O)_6]_{0.5}^+$, and a half (18-crown-6)-potassium, $[K(18\text{-c-}6)]_{0.5}^+$. These potassium cations are

(80) Flack, H. D.; Bernardelli, G. *Chirality* **2008**, *20*, 681–690.
(81) Flack, H. D.; Bernardelli, G. *Acta Crystallogr., Ser. A* **1999**, *55*, 908–915.
(82) Flack, H. D. *Acta Crystallogr., Ser. A* **1983**, *39*, 876–881.
(83) Addison, A. W.; Rao, T. N.; Reedijk, J.; van Rijn, J.; Verschoor, G. C. *J. Chem. Soc., Dalton Trans.* **1984**, 1349.

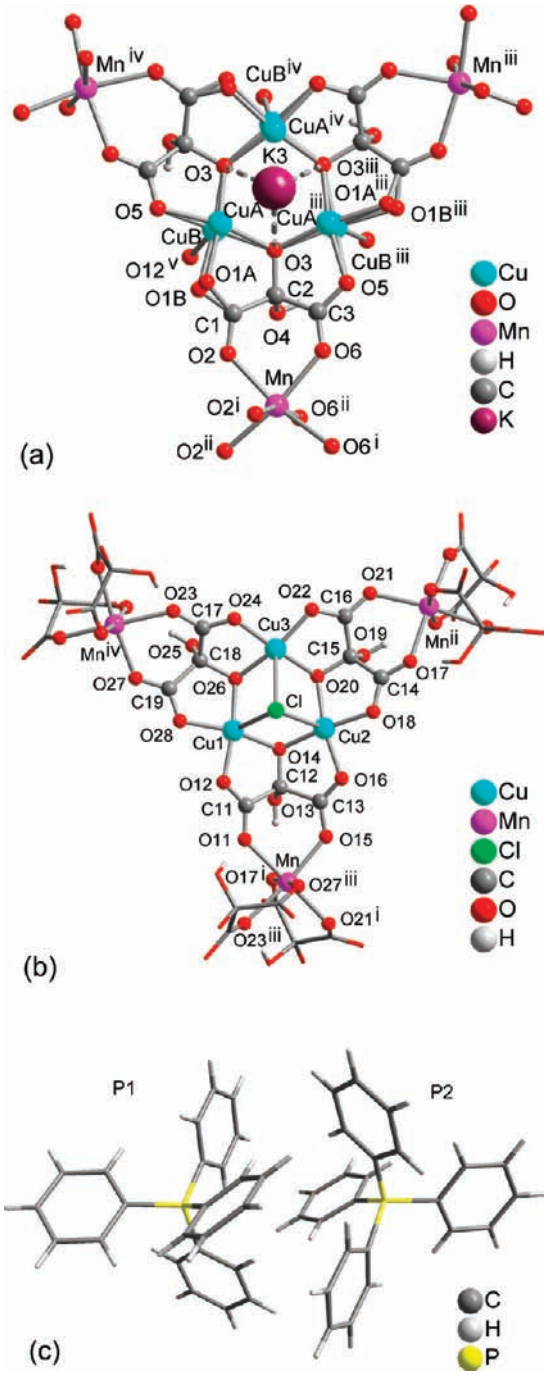

Figure 1. Cu_3 metalloligand and a manganese coordination sphere in (a) **1** and (b) **2** (with the 6-fold phenyl embrace of two Ph_4P^+ cations in a wire-frame mode in part c). Symmetry transformations and selected distances and angles are given in Tables 2 and 3. Shown for **1** is the 50:50 disorder to CuA and CuB and O1A and O1B (termed **1A** and **1B**, respectively, in the DFT calculations). The occurrence of a half-occupied K3 atom of $[K(18\text{-c-}6)]_{0.5}^+$ coincides with the CuB position.

severely disordered (see X-ray crystallography) and, thus, will not be discussed further.

The charge balance for the dinegative 3D framework (per formula unit) in **2** is derived by two symmetry-independent tetraphenylphosphonium, Ph_4P^+, ions (Figure 1c). These cations are located in the voids of the 3D anion framework (Figure 5).

The Ph_4P^+ cations are organized in a 3D supramolecular net through the expected 6-fold phenyl embrace (cf. Figures 1c and 6).[84−86] The sextuple phenyl embrace is a supramolecular attraction between Ph_3P moieties due

Table 2. Selected Bond Lengths (Å) and Angles (deg) in the Anion Net of **1**[a]

CuA−O1A	1.88(4)	CuB−O1B	1.96(4)
CuA−O3	1.927(9)	CuB−O3	1.913(10)
CuA−O3^{iv}	1.910(9)	CuB−O3^{iv}	1.958(9)
CuA−O5^{iv}	1.934(10)	CuB−O5^{iv}	1.949(10)
		CuB−O12^{v}	2.48(3)
Mn−O2	2.162(5)	Mn−O6	2.162(5)
K3−O3	3.102(8)		
O1A−CuA−O3	82.5(16)	O1B−CuB−O3	86.3(14)
O1A−CuA−O3^{iv}	168.9(12)	O1B−CuB−O3^{iv}	171.4(15)
O1A−CuA−O5^{iv}	89.7(15)	O1B−CuB−O5^{iv}	90.0(15)
O3−CuA−O3^{iv}	100.9(4)	O3−CuB−O3^{iv}	99.7(4)
O3−CuA−O5^{iv}	163.7(4)	O3−CuB−O5^{iv}	163.3(4)
O3^{iv}−CuA−O5^{iv}	84.2(2)	O3^{iv}−CuB−O5^{iv}	82.5(4)
CuA−O3−CuA^{iii}	117.1(4)	CuB−O3−CuB	138.6(4)
O2−Mn−O2^{i}	87.33(19)	O2−Mn−O6^{ii}	105.6(2)
O2−Mn−O6	82.78(18)	O6−Mn−O6^{i}	86.90(19)
O2−Mn−O6^{i}	163.26(19)		

[a] Symmetry transformations: i, y, z, x; ii, z, x, y; iii, $0.5 - y, -z, -0.5 + x$; iv, $0.5 + z, 0.5 - y, -x$; v, $x, 0.5 - y, -0.5 + z$.

Table 3. Selected Bond Lengths (Å) and Angles (deg) in the Anion Net of **2**[a]

Cu1−O12	1.908(10)	Cu3−O20	1.919(8)
Cu1−O14	1.972(8)	Cu3−O22	1.907(9)
Cu1−O26	1.927(9)	Cu3−O24	1.931(9)
Cu1−O28	1.912(10)	Cu3−O26	1.915(8)
Cu1−Cl	2.550(4)	Cu3−Cl	2.800(4)
Cu2−O14	1.922(8)	Mn−O11	2.175(9)
Cu2−O16	1.884(10)	Mn−O15	2.116(9)
Cu2−O18	1.926(10)	Mn−O17^{i}	2.138(9)
Cu2−O20	1.929(8)	Mn−O21^{i}	2.131(9)
Cu2−Cl	2.718(4)	Mn−O23^{iii}	2.147(9)
		Mn−O27^{iii}	2.084(10)
O12−Cu1−O14	85.9(4)	O20−Cu3−O22	84.3(4)
O12−Cu1−O26	171.0(4)	O20−Cu3−O24	176.1(4)
O12−Cu1−O28	88.7(4)	O20−Cu3−O26	97.7(4)
O14−Cu1−O26	98.1(3)	O22−Cu3−O24	93.1(4)
O14−Cu1−O28	156.0(4)	O22−Cu3−O26	160.9(4)
O26−Cu1−O28	84.4(4)	O24−Cu3−O26	83.8(4)
O12−Cu1−Cl	101.9(3)	O20−Cu3−Cl	81.9(3)
O14−Cu1−Cl	87.3(3)	O22−Cu3−Cl	119.3(3)
O26−Cu1−Cl	86.4(3)	O24−Cu3−Cl	101.9(3)
O28−Cu1−Cl	116.7(3)	O26−Cu3−Cl	79.7(3)
O14−Cu2−O16	86.1(4)		
O14−Cu2−O18	171.8(4)	O11−Mn−O15	85.6(4)
O14−Cu2−O20	98.7(4)	O11−Mn−O17^{i}	86.5(4)
O16−Cu2−O18	88.7(4)	O11−Mn−O21^{i}	172.2(4)
O16−Cu2−O20	163.7(5)	O11−Mn−O23^{iii}	87.1(3)
O18−Cu2−O20	84.6(4)	O11−Mn−O27^{iii}	90.9(4)
O14−Cu2−Cl	83.6(3)	O15−Mn−O17^{i}	90.7(3)
O16−Cu2−Cl	112.1(4)	O15−Mn−O21^{i}	94.2(3)
O18−Cu2−Cl	104.2(3)	O15−Mn−O23^{iii}	172.1(4)
O20−Cu2−Cl	84.0(3)	O15−Mn−O27^{iii}	92.8(4)
		O17^{i}−Mn−O21^{i}	85.7(4)
Cu2−O14−Cu1	110.9(4)	O17^{i}−Mn−O23^{iii}	91.7(4)
Cu3−O20−Cu2	118.0(5)	O17^{i}−Mn−O27^{iii}	175.5(4)
Cu3−O26−Cu1	115.9(4)	O21^{i}−Mn−O23^{iii}	93.4(3)
		O21^{i}−Mn−O27^{iii}	96.9(4)
τ-Cu1[b]	0.25	O23^{iii}−Mn−O27^{iii}	84.5(4)
τ-Cu2[b]	0.14		
τ-Cu3[b]	0.25		

[a] Symmetry transformations: i, $1.5 - x, 1 - y, 0.5 + z$; ii, $1.5 - x, 1 - y, -0.5 + z$; iii, $0.5 + x, 1.5 - y, 2 - z$; iv, $-0.5 + x, 1.5 - y, 2 - z$. [b] τ = Addison τ parameter.[83]

(84) Dance, I.; Scudder, M. L. *J. Chem. Soc., Chem. Commun.* **1995**, 1039–1040.

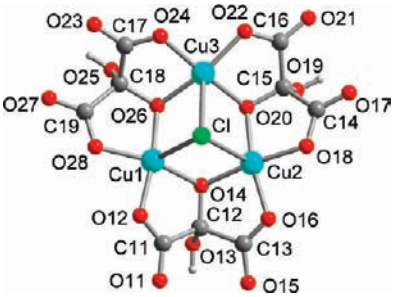

Figure 2. $\{Cu_3(C_3HO_6)_3Cl\}^{4-}$ metalloligand in **2**.

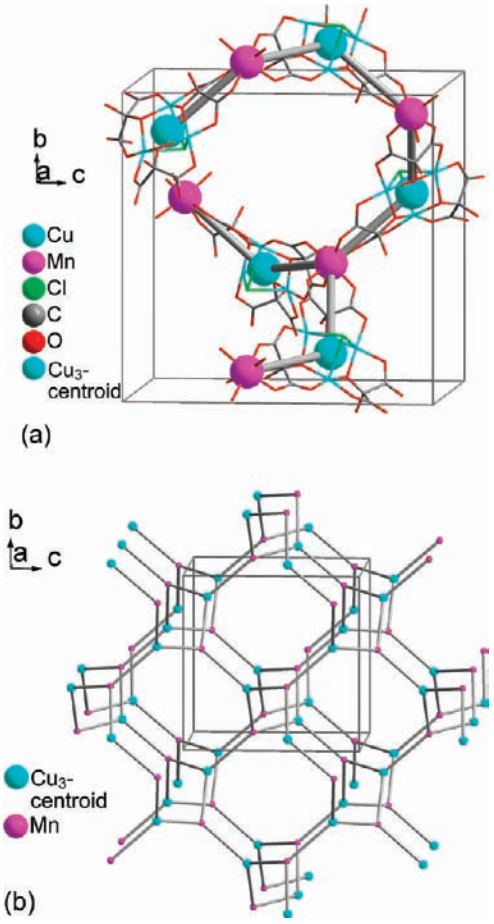

Figure 3. (a) Section of the 3D anion framework in **2** to indicate the development of (b) the $SrSi_2$ (10,3)-a topology through the connection of the manganese and Cu_3 centroid nodes. The four-membered helices are all left-handed (*M*).

to a concert of six attractive edge-to-face interactions between phenyl groups, has frequent occurrences in crystals, is usually centrosymmetric, and contributes an attraction of 60−85 kJ mol^{-1}.[84] This supramolecular 3D cation net (Figure 6) has the same $SrSi_2$, (10,3)-a topology as the anion framework, and both can be thought to form interpenetrating supramolecular and covalent (10,3)-a nets (Figure 7) as in $(Ph_3MeP)_2[NaCr(ox)_3]$.[87]

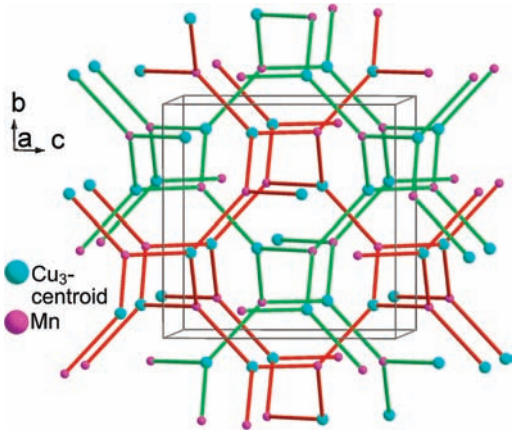

Figure 4. Interpenetration of the two symmetry-related nets in **1** by showing only the connection of the manganese and Cu_3 centroid nodes. The four-membered helices in the red net are right-handed (*P*) and those in the green net left-handed (*M*), which renders the combination of the two (10,3)-a nets racemic.

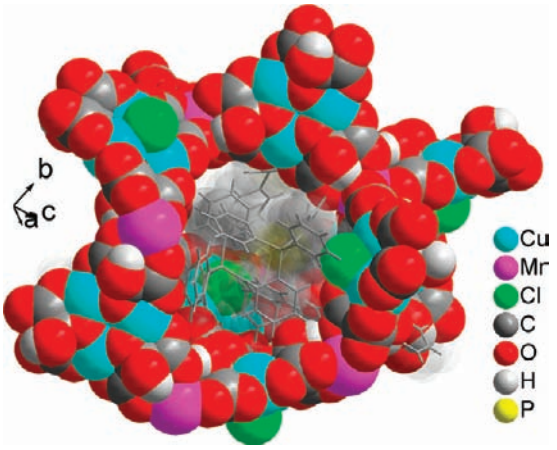

Figure 5. Section of the 3D anion framework in **2** in space-filling mode with two Ph_4P^+ cations (with a semitransparent van der Waals surface) in the void.

The cation and anion nets in **2** differ in their chirality when one traces the opposite handedness, for example, in the four-membered helices (Figure 7). Because of the different nature of the interpenetrated nets in **2** (different from **1**), the 3D (10,3)-a framework of **2** in the investigated crystal is chiral and enantiopure, thus crystallizing in the noncentrosymmetric Sohncke space group $P2_12_12_1$ (Table 2).[88,89] The homochirality arises from the solid-state packing in that the achiral $\{Cu_3(C_3HO_6)_3Cl\}^{4-}$ metalloligand assembles only manganese atoms of the same Λ configuration (cf. Figure 1).[37] The overall ensemble of the crystals in a batch of **2** can be expected to be racemic, that is, to contain crystals of Λ- and Δ-configured manganese atoms, respectively, in equal amounts.[90,91] In principle, they could be separated by hand here for crystals in the noncentrosymmetric crystal class 222 ($P2_12_12_1$),[92] in order to have enantiopure phases that may exhibit magnetochiral effects.[54]

(85) Dance, I.; Scudder, M. L. *Chem.—Eur. J.* **1996**, *2*, 481–486.
(86) Dance, I.; Scudder, M. L. *J. Chem. Soc., Dalton Trans.* **1996**, 3755–3769.
(87) Russell, V. M.; Craig, D. C.; Scudder, M. L.; Dance, I. G. *CrystEngComm* **2000**, *2*, 16–23.
(88) Flack, H. D. *Helv. Chim. Acta* **2003**, *86*, 905–921.
(89) Pidcock, E. *Chem. Commun.* **2005**, 3457–3459.
(90) Janiak, C.; Chamayou, A. C.; Uddin, A. K. M. R.; Uddin, M.; Hagen, K. S.; Enamullah, M. *Dalton Trans.* **2009**, 3698–3709.
(91) Enamullah, M.; Sharmin, A.; Hasegawa, M.; Hoshi, T.; Chamayou, A. C.; Janiak, C. *Eur. J. Inorg. Chem.* **2006**, 2146–2154.

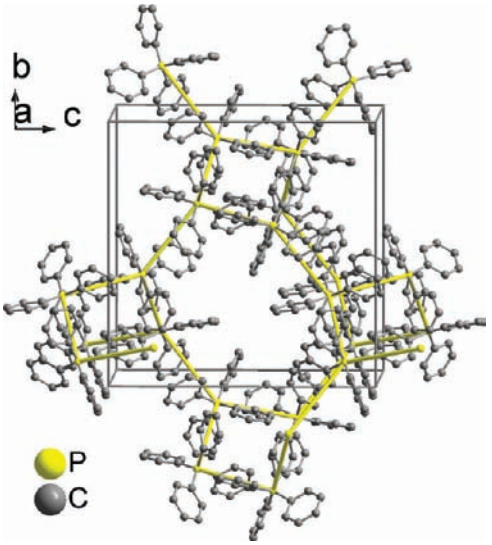

Figure 6. Supramolecular 3D net of the Ph_4P^+ cations in **2** through phenyl embraces (cf. Figure 1c) with the intermolecular P···P linkages (yellow lines), forming a (10,3)-a net.

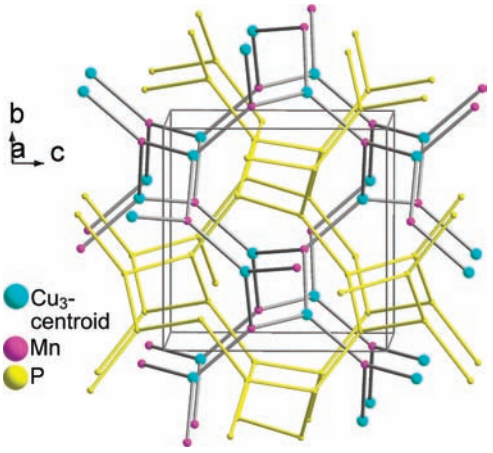

Figure 7. Interpenetration of the supramolecular cation (yellow) and covalent anion (gray lines) framework in **2** by showing only the connection of the phosphorus or manganese and Cu_3 centroid nodes, respectively. The four-membered helices in the cation net are right-handed (*P*) and those in the anion net left-handed (*M*), which renders the two (10,3)-a nets of opposite chirality.

There is an orientational disorder of the spherical Ph_4P^+ cations that affects the overall crystal and dataset quality. Also found in the voids is a water molecule of crystallization (O1W; cf. Figure 1), which is within a hydrogen-bonding distance of O14 and O26 (O1W···O14 2.959 Å and O1W···O26 3.101 Å).

Magnetic Properties. The thermal dependence of the $\chi_M T$ product for **1** is typical for copper(II)−manganese-(II) compounds with ferrimagnetic coupling that order magnetically below a critical temperature (Figure 8)[93−96] [χ_M is the magnetic susceptibility for a $Cu^{II}{}_3Mn^{II}$ system, in agreement with the chemical formula of compound **1**, and T the temperature].

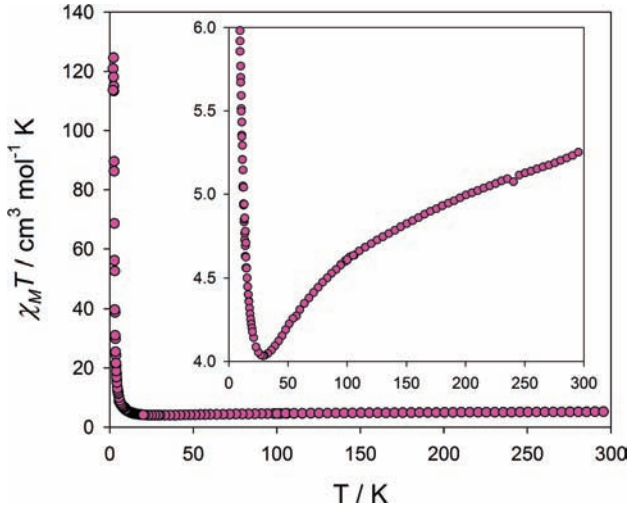

Figure 8. Thermal dependence of the $\chi_M T$ product for **1**. The inset corresponds to the same plot in a smaller scale in order to show the minimum of the $\chi_M T$ product characteristic of ferrimagnetic materials.

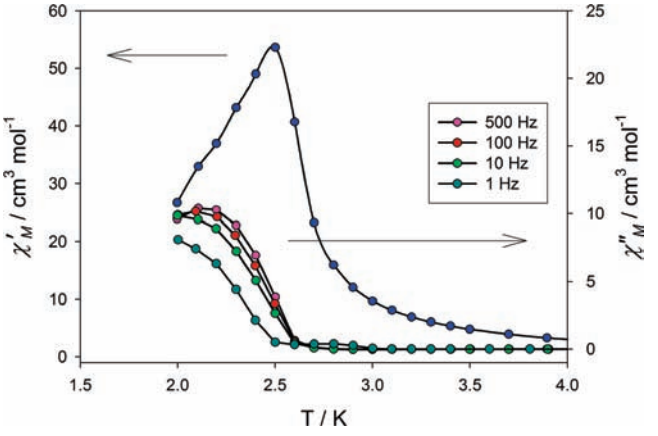

Figure 9. Thermal dependence of the in-phase (blue dots), χ_M', and out-of-phase, χ_M'', molar magnetic susceptibilities at different frequencies of the oscillating field for compound **1**. The solid lines are eye guides.

At room temperature, $\chi_M T$ is 5.1 cm^3 mol^{-1} K, a value that is lower than expected for a Mn^{II} ion and three uncoupled Cu^{II} ions [$\chi_M T = 3(N\beta^2 g^2{}_{Cu}/3k)S_{Cu}(S_{Cu}+1) + (N\beta^2 g^2{}_{Mn}/3k)S_{Mn}(S_{Mn}+1) = 5.6$ cm^3 mol^{-1} K with $g_{Cu} = 2.10$, $S_{Cu} = {}^1/_2$, $g_{Mn} = 2.0$, and $S_{Mn} = {}^5/_2$].[11] It continuously decreases to reach a minimum value of 4.0 cm^3 mol^{-1} K at 30 K, and then there is a sharp increase that leads $\chi_M T$ to reach values above 100 cm^3 mol^{-1} K, decreasing again at lower temperatures due to saturation effects. The long-range magnetic ordering is confirmed by the ac magnetic susceptibility measurements (Figure 9).

χ_M'' has nonzero values at temperatures lower than 2.5 K, and the maximum slightly shifts to higher values at higher frequencies that imply a certain degree of spin-glass

(92) Klapper, H.; Hahn, T. *International Tables for Crystallography Vol. A*, 5th ed.; Kluwer: Dordrecht, 2002; Chapter 10.2, Table 10.2.1.1, pp 804 and 805.
(93) Pardo, E.; Ruiz-Garcia, R.; Lloret, F.; Faus, J.; Julve, M.; Journaux, Y.; Novak, M. A.; Delgado, F. S.; Ruiz-Perez, C. *Chem.—Eur. J.* **2007**, *13*, 2054–2066.
(94) Kahn, O.; Pei, Y.; Verdaguer, M.; Renard, J. P.; Sletten, J. *J. Am. Chem. Soc.* **1988**, *110*, 782.
(95) Stump, H. O.; Pei, Y.; Ouahab, L.; Leberre, F.; Codjovi, E.; Kahn, O. *Inorg. Chem.* **1993**, *32*, 5687.
(96) Stump, H. O.; Pei, Y.; Kahn, O.; Sletten, J.; Renard, J. P. *J. Am. Chem. Soc.* **1993**, *115*, 6738.

Scheme 5. Schematic View of the Mn−Cu, J_2, and Cu−Cu, J_1, Magnetic Couplings

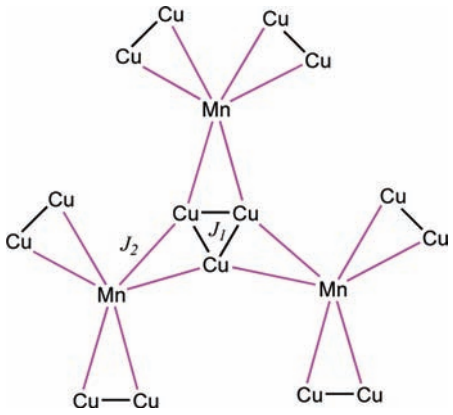

behavior of the magnetically ordered state.[97−99] Compound **1** behaves as a soft magnet with a very small cohercitive field, as can be seen in the hysteresis loop (Figure S2 in the Supporting Information). However, compound **1** is not a typical manganese(II)−copper(II) ferrimagnet because the Cu^{II} ions build μ-alkoxo-bridged equilateral triangles and each Mn^{II} ion is surrounded by three copper(II) triangles in such a way that each Mn^{II} interacts directly with two Cu^{II} ions from each triangle through anti−anti carboxylate bridges. At the same time, the Cu^{II} ions are also magnetically coupled through the μ-alkoxo bridges within the triangle. This situation has no precedents and needs to be analyzed in detail. We can draw a magnetic coupling scheme with two different magnetic coupling constants, J_1 and J_2 (Scheme 5).

J_2 refers to the manganese(II)−copper(II) coupling through the anti−anti carboxylate bridges, and J_1 refers to the copper(II)−copper(II) coupling through the μ-alkoxo bridges. Depending on their intensity and their ferro- or antiferromagnetic nature, four different situations can be displayed, FF, FAF, AFF, and AFAF, for J_1 and J_2, respectively. In order to understand the magnetic behavior of **1**, we need to set a starting hypothesis. It can certainly be assumed for the manganese(II)−copper(II) interaction to be antiferromagnetic ($J_2 < 0$, AF),[93−96] but, in principle, J_1 can be left without restrictions. Magnetically coupled copper(II) cyclic trinuclear systems with C_3 symmetry (at Heisenberg, Dirac, and Van Vleck levels) display three electronic states: a quartet ($S = {}^3/_2$, $^4A_2$) and a doubly degenerated doublet ($S = {}^1/_2$, ^2E).[21,24,30] If J_1 is negative, the ^2E $S = {}^1/_2$ would be the ground state; on the other hand, if J_1 is positive, the $^4A_2$ $S = {}^3/_2$ would be the ground state. Magnetic ordering is reached at very low temperatures, so the Mn^{II} ions will interact with the electronic ground state of the trinuclear system, either ${}^3/_2$ or ${}^1/_2$. Thus, it is important to distinguish whether the ${}^3/_2$ or ${}^1/_2$ state is lower in energy.

(97) Branzea, D. G.; Sorace, L.; Maxim, C.; Andruh, M.; Caneschi, A. *Inorg. Chem.* **2008**, *47*, 6590–6592.
(98) Bellouard, F.; Clemente-León, M.; Coronado, E.; Galán-Mascarós, J. R.; Gómez-García, C. J.; Romero, F.; Dunbar, K. *Eur. J. Inorg. Chem.* **2002**, 1603–1606.
(99) Omerzu, A.; Mertelj, T.; Demsar, J.; Mihailovic, D.; Drobac, D.; Prester, M. In *Introduction to Physical Techniques in Molecular Magnetism: Structural and Macroscopic Techniques*; Palacio, F., Ressouche, E., Schweizer, J., Eds.; Servicio de Publicaciones de la Universidad de Zaragoza: Zaragoza, Spain, 1999; pp 93 and 94.

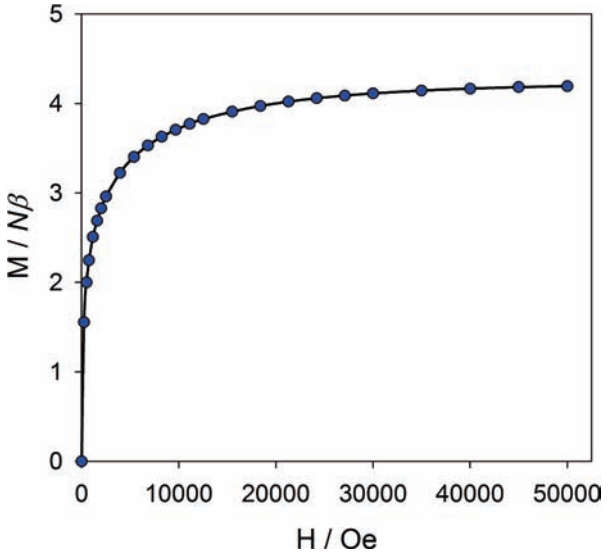

Figure 10. Field dependence of magnetization for compound **1** at 2 K. The solid line is an eye guide.

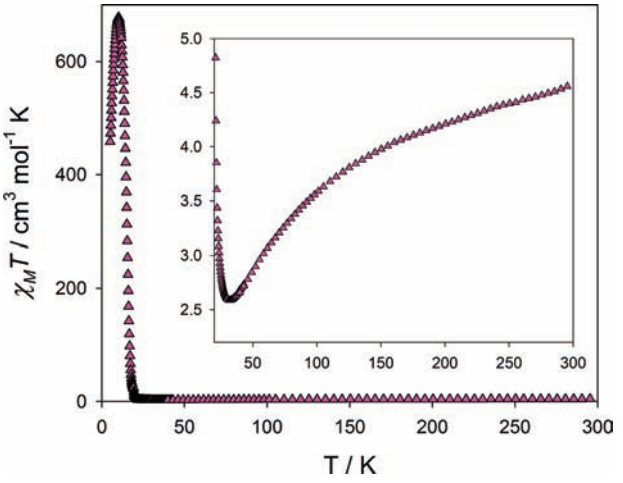

Figure 11. Thermal dependence of the $\chi_M T$ product for **2**. The inset corresponds to the same plot in a smaller scale in order to show the minimum of the $\chi_M T$ product characteristic of ferrimagnetic materials.

The M vs H plot for **1** shows a magnetization value at 50.000 Oe of ca. 4.0 $N\beta$ that arises from a total spin of $S = 2$, which is consistent with an antiferromagnetic coupling between a HS Mn^{II} ion ($S_{Mn} = {}^5/_2$ with $g = 2.0$) and $S = {}^1/_2$ for the trinuclear unit ($g_{Cu3} \approx 2.1$) [$M_S = (2 \times {}^5/_2) - (2.1 \times {}^1/_2) \approx 4.0\ N\beta$] (Figure 10). Thus, looking at the M vs H plot, the Cu^{II} ions are antiferromagnetically coupled within the triangle, displaying a $S_T = {}^1/_2$ spin ground state. Also, this $S_T = {}^1/_2$ entity is antiferromagnetically coupled with its Mn^{II} nearest neighbors. Another experimental fact pointing in this direction is the minimum value of the $\chi_M T$ product in the $\chi_M T$ vs T plot of **1** (Figure 8). This value is 4.0 cm^3 mol^{-1} K, which coincides with the minimum value observed for the ferrimagnetically coupled $S = {}^5/_2$ and ${}^1/_2$ systems.[93−96]

The thermal dependence of the $\chi_M T$ product for compound **2** shows a shape similar to that of **1** and also points toward a ferrimagnetic interaction among the manganese(II) and copper(II) trinuclear units, which leads to a long-range ferrimagnetic ordering (Figure 11). The χ_M vs

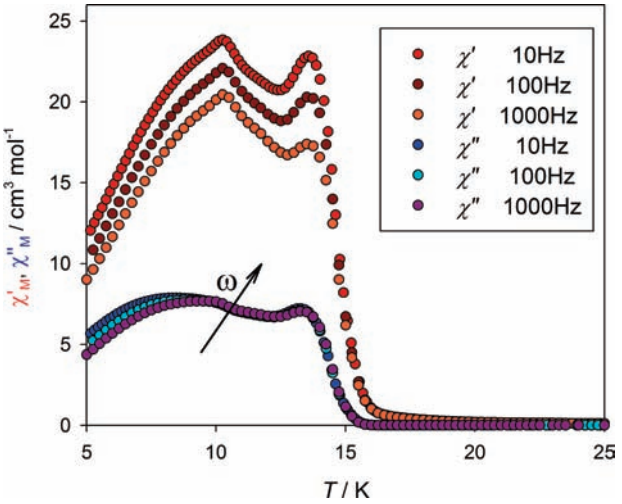

Figure 12. Thermal dependence of the in-phase (red ●, maroon ●, and orange ●), χ_M', and out-of-phase (blue ●, teal ●, and purple ●), χ_M'', magnetic susceptibilities at different frequencies of the oscillating field for **2**.

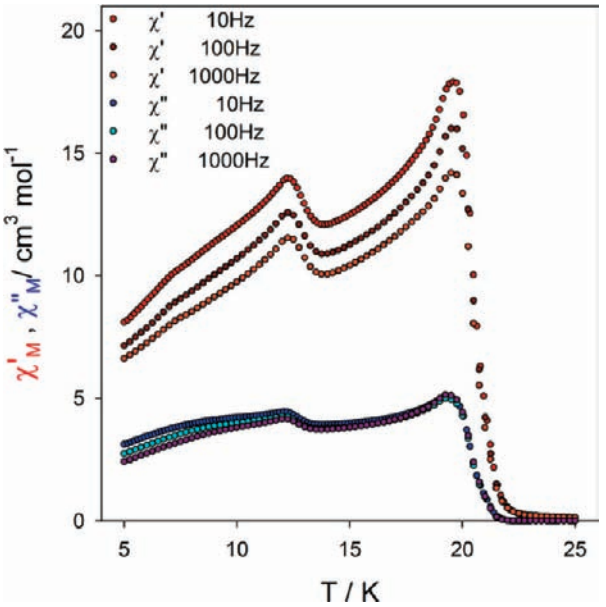

Figure 13. Thermal dependence of the in-phase (red ●, maroon ●, and orange ●), χ_M', and out-of-phase (blue ●, teal ●, and purple ●), χ_M'', magnetic susceptibilities at different frequencies of the oscillating field for **2B**.

T plot (Figure S3 in the Supporting Information) displays a sigmoidal shape with onset of the long-range magnetic ordering process around 15 K. The ac magnetic measurement confirms the long-range ordering showing a T_c of 15.2 K and a broad peak at around 8−10 K that can be assigned to a spin-glass transition of the ferrimagnetically ordered state as the maximum in χ_M'' shifts to higher values at higher frequencies (Figure 12).[97−100]

An undetermined number of crystallization water molecules of **2** can be removed by means of a soft vacuum at room temperature, yielding the dehydrated phase, **2B**. The thermal dependences of the $\chi_M T$ product and the *M* vs *H* plot at 2 K of **2B** are almost identical with those of **2** (Figures S4 and S5 in the Supporting Information, respectively). However, the ac magnetic measurements show an increase of the T_c, becoming 21.5 K (Figure 13). The maximum at 13 K suggests that the conversion of **2** to **2B** is not complete. Also, the reentrance to the spin-glass phase is still observed at temperatures below 10 K.

The hysteresis loop of **2** at 2 K shows a coercive field of 100 Oe; thus, compound **2** can be classified as a soft magnet (Figure 14). The magnetization of compound **2** in the *M* vs *H* plot reaches a value of 1.8 $N\beta$ at 50 000 Oe, much smaller than that reached by compound **1**. This can be explained by assuming that the HS state is the ground state for the trinuclear unit in the magnetically ordered phase of **2**. With that approach, we would have $M_S = (2.0 \times {}^5/_2) - (2.15 \times {}^3/_2) = 1.78\ N\beta$, which coincides with the experimental value. The very low value of the $\chi_M T$ product at the minimum in the $\chi_M T$ vs *T* plot supports this hypothesis too.

DFT Calculations. The copper(II) trinuclear unit displays a doublet and a quartet ground state in **1** and **2**, respectively. This situation can be explained by assuming an antiferromagnetic coupling for the trinuclear units in **1**, $J < 0$, and a ferromagnetic coupling for those in **2**, $J > 0$. Because of the 3D structure of both compounds, the determination of the values of the magnetic coupling constants cannot be performed from magnetic susceptibility measurements. However, they can be estimated in fragments of the structures of **1** and **2** containing the copper(II) trinuclear units by means of DFT calculations. Moreover, when this study is extended, it may be possible to estimate which parameters dominate the magnetic coupling and to which extent they are important in order to explain/understand the magnetic behavior of the copper(II) trinuclear unit.

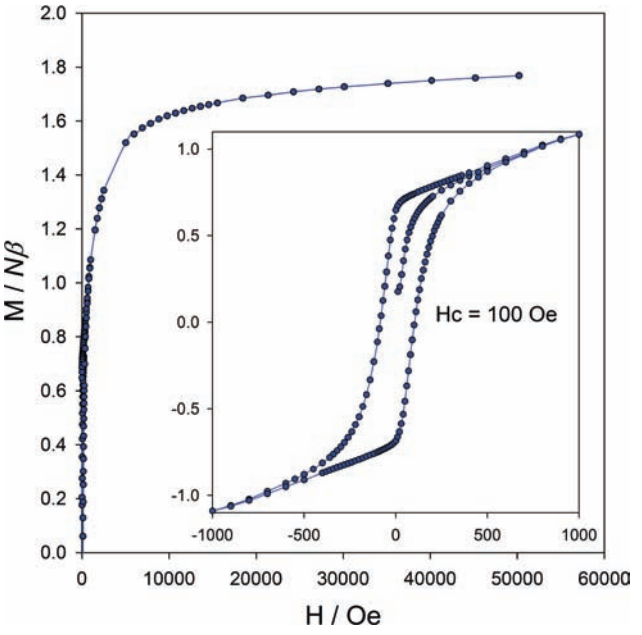

Figure 14. Field dependence of magnetization for compound **2** at 2 K. The inset shows the hysteresis loop at 2 K. The solid line is an eye guide.

The starting point consists of calculation of the magnetic coupling constant of the trinuclear units in **1** and **2**. The $[Cu_3(Hmesox)_3]^{3-}$ and $[Cu_3(Hmesox)_3Cl]^{4-}$ anionic fragments were considered for **1** and **2**, respectively (Figures 1a and 2). Compound **1** contains two different

(100) Coronado, E.; Galán-Mascarós, J. R.; Martí-Gastaldo, C.; Waerenborgh, J. C.; Gaczynski, P. *Inorg. Chem.* **2008**, *47*, 6829–6839.

Table 4. Selected Structural, Energetic, and Magnetic Features of the Trinuclear Units **1A**, **1B**,[a] and **2**[b]

		1A		**1B**		**2**[a]	
Cu−O−Cu, θ/deg		117.1(4)		138.6(4)		113.6	
hinge distortion, γ/deg		20.5(2)		20.0(2)		26.36	
τ/deg		3.3(2)		3.3(2)		1.7	
distance Cu−Cl						2.64	
E_{HS}/hartree	$\langle S^2\rangle$	−6620.5791988	3.76	−6620.5540960	3.76	−7080.487956	3.75
E_{BS}/hartree	$\langle S^2\rangle$	−6620.5796617	1.74	−6620.5565300	1.70	−7080.487973	1.75
J/cm^{-1}		−101		−534		−3.8	

[a] Trinuclear unit **1A** contains CuA and O1A, unit **1B** CuB and O1B, respectively (cf. Fig. 1a). [b] These values correspond to the idealized fragment of compound **2**; see the text.

trinuclear units, **1A** and **1B** (cf. Fig. 1a). Single-point calculations were performed for both fragments. The selected fragments of **1** already have C_3 symmetry, and their atomic coordinates were taken directly from the crystal structure file. For such a system, the magnetic coupling constant could be obtained from the energies of the HS and BS, low-spin, configurations, $J = -(E_{HS} - E_{BS})$, as explained in the Experimental Section.[24]

The original trinuclear unit of **2** is less symmetric, C_1, having three different Cu^{II} atoms and three different Cu−O_b−Cu bridging angles that span in the range 110.9(4)−118.0(5)° (Table 3). Also, the three different Cu^{II} ions have three different basal planes that have different hinge distortions, spanning in the range 21.6−27.4°. This situation would lead to three different magnetic coupling constants (J_{12}, J_{23}, and J_{13}) and would make it impossible to get a solution.[101,102] In order to solve this problem, the structure of the molecule has been idealized, imposing the C_3 symmetry.[20] For such a purpose, the three Cu−O_b−Cu angles were made equal to 113.6°, and deviations from the planarity, γ, were made equal to 26.36°, which are average values of the original ones (see Table S2 in the Supporting Information for details). In this way, the previous equation can also be used to obtain a magnetic coupling constant that has to be assumed as a mean value of the magnetic coupling constants operating in the trinuclear unit of **2**. This should not be a major problem because the objective of this study is to analyze the trend and the influence of some structural parameters more than the determination of the exact value of the magnetic coupling constants that, actually, cannot be obtained from experimental measurements.

Table 4 gives the total energies, E_{HS} and E_{BS}, the $\langle S^2\rangle_{HS}$ and $\langle S^2\rangle_{BS}$, and the magnetic coupling constant, J, calculated as mentioned for each fragment. We observe a strong antiferromagnetic coupling for the Cu_3 units in **1A** and **1B** and a weak antiferromagnetic coupling between the Cu^{II} ions in the idealized unit of **2**, $J = -3.8$ cm^{-1}. Then, the DFT calculations validate the hypothesis of the low-spin configuration for the ground state in the Cu_3 fragments of **1** and a HS configuration can be expected for that of **2**. [A weak antiferromagnetic coupling can lead to an apparent HS ground state in **2** because it may become frustrated by the stronger manganese(II)−copper(II) antiferromagnetic coupling through the anti−anti carboxylate bridge that would stabilize the HS ground state in the Cu_3 unit.] The

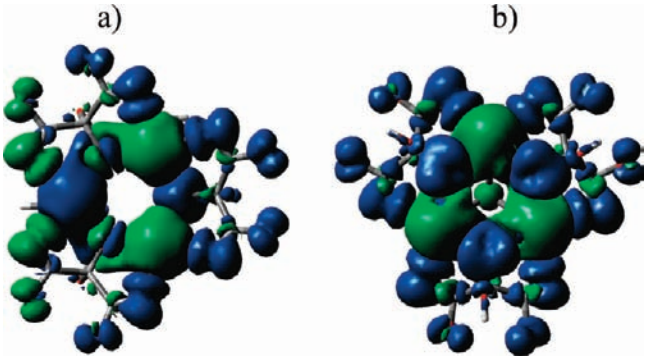

Figure 15. Isosurfaces of the spin densities for the (a) BS and (b) HS states in **1A** and **2**, respectively.

spin-density distributions of the BS $M_S = {}^1/_2$ and $S = {}^3/_2$ states of the trinuclear units of **1A** and **2**, respectively, are shown in Figure 15.

It is clearly observed that the Cu^{II} ions exhibit an $\alpha\alpha\beta$ spin distribution in the BS state for **1A** (α and β refer to up and down spins, respectively) and that the spin distribution in that fragment does not have C_3 symmetry. The spin density is not localized on the Cu^{II} ions, but it is delocalized all around the fragment. The two bridging oxygen atoms that antiferromagnetically couple the Cu^{II} ions have positive and negative spin densities, whereas the one that ferromagnetically couples two of them exhibits only the opposite sign to those of the copper atoms. The carboxylate groups have important spin densities, which ensures transmission of the magnetic coupling outside the fragment. However, distribution of the spin density in the trinuclear core introduces a certain degree of frustration in the transmission of the magnetic effect along the crystal structure because two of the three Mn^{II} ions surrounding each trinuclear unit interact with two Cu^{II} ions of different spin orientation (Scheme 6a).

In this situation, the Mn^{II} ions cannot adopt an antiferromagnetic orientation toward all of the Cu^{II} ions simultaneously. This produces a fragmentation of the magnetic network that makes an increase of the magnetic correlation difficult, and this can be the reason for the much lower critical temperature of **1**. On the other hand, the cyclic trinuclear fragment in **2** has C_3 symmetry for the $S = {}^3/_2$ "ground" state (Figure 13b). The spin density is highly delocalized toward the carboxylate groups, and all of them exhibit the same sign. The copper(II)−manganese(II) antiferromagnetic (or ferrimagnetic) coupling is easily transmitted along the 3D covalent network, leading to a much higher ordering temperature, as was experimentally observed (Scheme 6b).

(101) Ruiz, E.; Alemany, P.; Alvarez, S.; Cano, J. *J. Am. Chem. Soc.* **1997**, *119*, 1297–1303.
(102) Pardo, E.; Bernot, K.; Julve, M.; Lloret, F.; Cano, J.; Ruiz-García, R.; Delgado, F. S.; Ruiz-Pérez, C.; Ottenwaelder, X.; Journaux, Y. *Inorg. Chem.* **2004**, *43*, 2768–2770.

Scheme 6. Magnetic Coupling of the LS (a) and HS (b) Trinuclear Units with the Mn^{II} Ions[a]

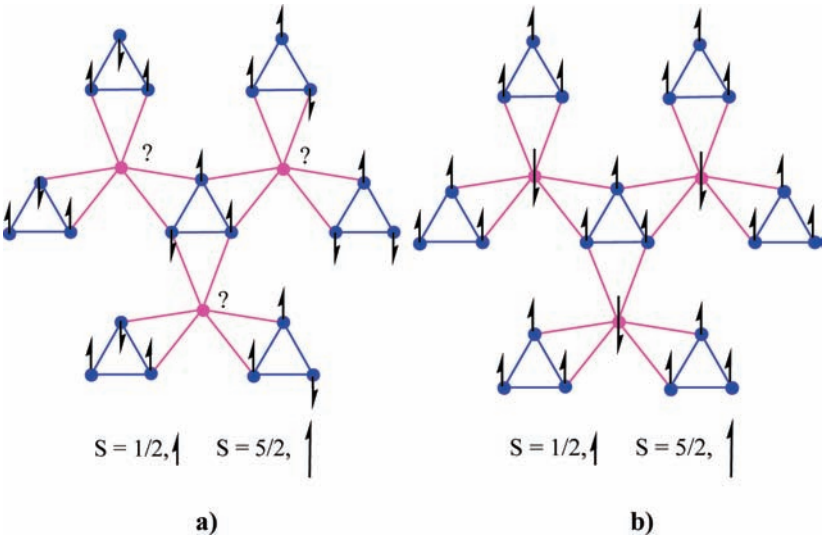

[a] The LS configuration yields frustrated Mn^{II} ions and a frustration in the transmission of the magnetic effect along the three dimensions of the crystals.

The plots of the singly occupied molecular orbitals (SOMOs) for the HS and BS configurations of the trinuclear units of **1** and **2** are shown in Figure S6 in the Supporting Information. The $d_{x^2-y^2}$ character of the Cu^{II} orbitals is clearly observed in the SOMOs of either the doublet or quartet state in all of the fragments. This is in agreement with the square-planar and pyramidal environments of the Cu^{II} ions in **1** and **2**, respectively.

The different magnetic behavior of **1** and **2** must be explained in terms of different structural parameters occurring in both trinuclear units. The main structural factors governing the magnetic coupling among Cu^{II} ions through alkoxo-bridging groups are the $Cu-O_b-Cu$ bridging angles (θ), the angle subtended by the equatorial planes of the Cu^{II} ions with those of the three bridging oxygen atoms (γ, hinge distortion), the deviation from this plane of the $C-O_b$ bond (τ), and also the geometry of the Cu^{II} ion environment (Figure S7 in the Supporting Information).[101] All sets of parameters were calculated for both **1A** and **1B** units occurring in compound **1** and for compound **2** (Table 4).

Alkoxo-bridged copper(II) dinuclear complexes display antiferromagnetic couplings for large $Cu-O_b-Cu$ bridging angles, in such a way that the larger the angle, the stronger the antiferromagnetic coupling.[103] Small deviations from planarity (low γ and τ values) also reinforce the antiferromagnetic coupling.[101] This behavior can also be expected for the cyclic trinuclear clusters; thus, the antiferromagnetic coupling is expected to be much more intense in **1**, which has larger $Cu-O_b-Cu$ angles, stabilizing the doublet ground state. It has been observed that the compound $Na_3[Cu_3(mal)_3(H_2O)]\cdot 8H_2O$ (H_2mal = malic acid) exhibits $J = -258\ cm^{-1}$ for a mean Cu−O−Cu angle of 134.0(6)°.[28] On the other hand, the smaller $Cu-O_b-Cu$ angle and the larger hinge distortion in **2** stabilize the ferromagnetically coupled HS state.[101] [The effect of τ seems to be frustrated by a stronger influence of θ and γ because the former points toward stronger ferromagnetic coupling in **1**, which is not observed.]

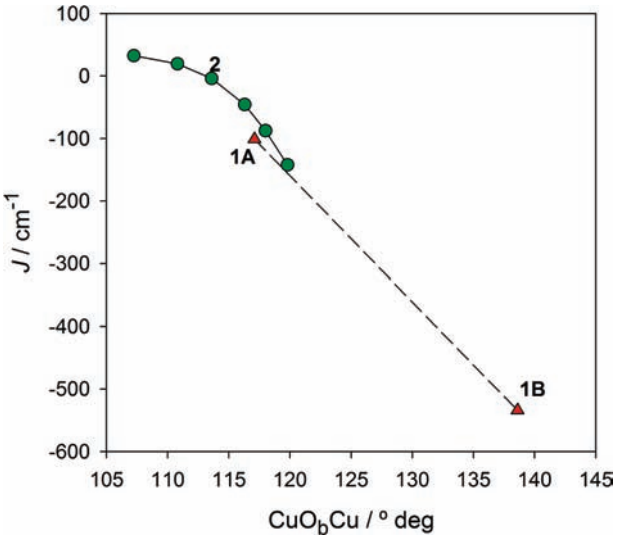

Figure 16. Dependence of the magnetic coupling constant, J, on the bridging Cu−O−Cu angle in the fragment of **2** (see the text). **1A** and **1B** are also represented.

Looking at Table 4, we observe that the calculated magnetic coupling constants span a very wide range, from −3.8 to $-534\ cm^{-1}$. This variation must be related to variation of some structural parameters. From those represented in Table 4, it can be seen that γ and τ have much lower variation than θ. Thus, without discarding the influence of the former parameters, we analyzed by means of a DFT study the dependence of the magnetic coupling constant with the $Cu-O_b-Cu$ bridging angle in the trinuclear units of **1** and **2** (Figure 16). The C_3 symmetry was imposed to the idealized fragment of **2**, and then the bridging oxygen atoms were displaced from their original positions to reach the desired θ angles. The θ values were varied in a narrow range in order to avoid large deviations from the starting structures (A more

(103) Crawford, V. H.; Richardson, H. W.; Wasson, J. R.; Hodgson, D. J.; Hatfield, W. E. *Inorg. Chem.* **1976**, *15*, 2107.

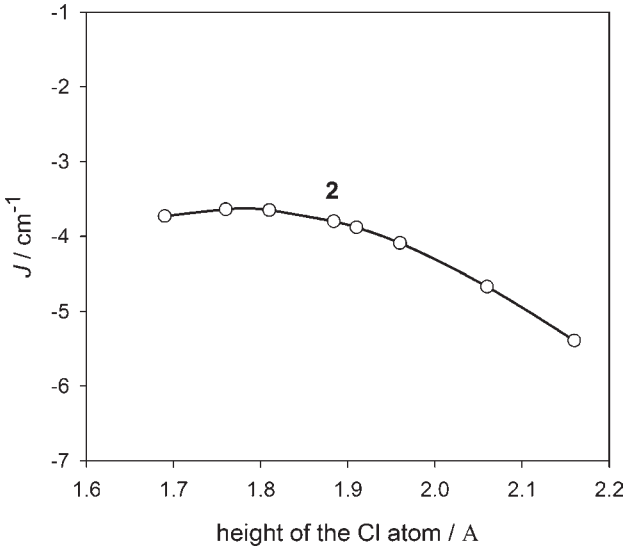

Figure 17. Dependence of the magnetic coupling constant, J, with the height of the μ_3-chlorine atom in the idealized fragment of **2**.

detailed description of the procedure is given in the Supporting Information.)

The magnetic coupling constant follows the general trend exhibited by copper(II) hydroxo-bridged dinuclear complexes with stronger antiferromagnetic couplings for larger bridging angles, with ferromagnetic coupling occurring for angles smaller than ~112°. The result of this study compares well with the result obtained for the fragment **1A**, which has similar structural parameters. Planar dihydroxo-bridged copper(II) dinuclear complexes exhibit ferromagnetic coupling for angles lower than 98°;[103] the ferromagnetic coupling occurs at larger angles in our compounds probably because of the hinge distortion exhibited by the trinuclear unit in **2**.

Compound **1** gives the opportunity to study the dependence of the magnetic coupling constant with θ, keeping the rest of parameters unchanged. The **1A** and **1B** units accidentally have almost the same hinge distortion and τ, differing mainly in the Cu−O_b−Cu angle (Table 4). It can also be observed that the stronger antiferromagnetic coupling occurs in the fragment **1B** with a larger θ angle.

It is very appealing that the trinuclear cluster of **2** mixes the two proposed limiting structures for the native intermediate of the active sites of the multicopper oxidases.[24,30] Solomon and co-workers studied the electronic and magnetic properties of some μ_3-oxo-bridged trinuclear copper(II) systems, and they observed that the height of the μ_3-oxo group with respect to the Cu_3 plane was of capital importance. In order to investigate whether our systems have similar behavior, we studied the dependence of J with the μ_3-Cl^--to-Cu_3 plane distance (Figure 17).

The original distance is 1.88 Å, and we varied it in the range 1.68−2.13 Å. For such a purpose, the location of the chloride ion was moved above and below its original position, leaving the rest of the molecule unchanged. It can be observed that, in contrast to the result obtained by Solomon and co-workers, in our case, the location of μ_3-Cl^- has little influence. This could be due to the different geometries of the copper(II) environment in both cases. The molecule studied by Solomon and co-workers has a trigonal-bipyramidal environment for the Cu^{II} ions, with a magnetic orbital with d_{z^2} character,[24] whereas in our case, the pyramidal geometry leads to a magnetic orbital with $d_{x^2-y^2}$ character with little spin density in the apical position filled by the chloride ion. Thus, the copper(II) environment seems to be determinant of the nature of the magnetic coupling through the μ_3-Cl^- atom.

Conclusions

Two new molecule-based magnets were prepared from the same SBU, $[Cu_3(Hmesox)_3]^{3-}$. This SBU acts as a planar 3-connecting node and, combined with the 3-connected Mn^{2+} node, yields the anionic chiral 3D $[MnCu_3(Hmesox)_3]^-$ (10,3)-a network. For the charge balance, different countercations were incorporated into the network, leading to different crystal structures. Compound **1** yielded a doubly interpenetrated network with both *P* and *M* (10,3)-a anionic nets in a racemic centrosymmetric crystal structure and the disordered $[K(H_2O)_6]^+$ and $[K(18\text{-crown-}6)]^+$ cations in the small holes. On the other hand, the incorporation of Cl^- to the $[Cu_3(Hmesox)_3]^{3-}$ metalloligand and Ph_4P^+ as cations yielded crystals of **2** with spontaneous resolution of $[MnCu_3(Hmesox)_3Cl]^{2-}$ into homochiral *P* or *M*, respectively, anionic (10,3)-a nets in a single crystal. The Ph_4P^+ cations filled the voids in the covalent anionic net, thereby forming a supramolecular net through phenyl embrace. The P···P linkages built a (10,3)-a net of opposite handedness to the covalent net.

Compounds **1** and **2** order magnetically below 2.5 and 15.2 K, respectively. This shows the efficient transmission of the magnetic interaction by means of the carboxylate groups of the mesoxalato ligands. A dehydrated phase of **2** exhibits a T_c of 21.8 K. Saturation of the magnetization points toward $S = {}^1/_2$ and ${}^3/_2$ spin ground states for $[Cu_3(Hmesox)_3]^{3-}$ in **1** and **2**, respectively. A DFT study performed in fragments of both compounds supports this hypothesis. The structural parameters governing the HS or LS configuration of the ground state were investigated also by DFT, and we can conclude that the main factor is the Cu−O−Cu bridging angle θ, with the height of the chloride ion in **2** being much less important. However, the μ_3-Cl^- ion on top of the three Cu^{II} ions maximized the hinge distortion and minimized the Cu−O−Cu angle, leading to a ferromagnetic-like ground state.

Acknowledgment. J.S. acknowledges financial support from the Ministerio Español de Ciencia e Innovación through Project MAT2007-60660 and "Factoría de Cristalización" (Consolider-Ingenio2010, CSD2006-00015). C.J. thanks the German Science Foundation for support through Grant Ja466/14-1/2.

Supporting Information Available: Computational details of the study of the dependence of the magnetic coupling constant on the Cu−O−Cu bridging angle, calculated energies and Cartesian coordinates of the input files of the DFT study, full reference of the *Gaussian03* code, and crystallographic data in CIF format of the reported structures, 781994 and 781995. This material is available free of charge via the Internet at http://pubs.acs.org. The atomic coordinates for these structures have also been deposited with the Cambridge Crystallographic Data Centre. The coordinates can be obtained, upon request, from the Director, Cambridge Crystallographic Data Centre, 12 Union Road, Cambridge CB2 1EZ, U.K.